JCI insight

RESEARCH ARTICLE

Deletion of p22^{phox}-dependent oxidative stress in the hypothalamus protects against obesity by modulating β_3-adrenergic mechanisms

Heinrich E. Lob,[1] Jiunn Song,[1] Chansol Hurr,[2] Alvin Chung,[1] Colin N. Young,[1,2] Allyn L. Mark,[3,4] and Robin L. Davisson[1,4]

[1]Department of Biomedical Sciences, College of Veterinary Medicine, Cornell University, Ithaca, New York, USA. [2]Department of Pharmacology and Physiology, George Washington University, School of Medicine and Health Sciences, Washington, DC, USA. [3]Department of Internal Medicine, Carver College of Medicine, University of Iowa, Iowa City, Iowa, USA. [4]Department of Cell and Developmental Biology, Weill Cornell Medical College, New York, New York, USA.

A role for oxidative stress in the brain has been suggested in the pathogenesis of diet-induced obesity (DIO), although the underlying neural regions and mechanisms remain incompletely defined. We tested the hypothesis that NADPH oxidase–dependent oxidative stress in the paraventricular nucleus (PVN), a hypothalamic energy homeostasis center, contributes to the development of DIO. Cre/LoxP technology was coupled with selective PVN adenoviral microinjection to ablate *p22^{phox}*, the obligatory subunit for NADPH oxidase activity, in mice harboring a conditional *p22^{phox}* allele. Selective deletion of *p22^{phox}* in the PVN protected mice from high-fat DIO independent of changes in food intake or locomotor activity. This was accompanied by β_3-adrenoceptor–dependent increases in energy expenditure, elevations in brown adipose tissue thermogenesis, and browning of white adipose tissue. These data reveal a potentially novel role for brain oxidative stress in the development of DIO by modulating β_3-adrenoceptor mechanisms and point to the PVN as an underlying neural site.

Introduction

The central nervous system (CNS) is critical for the control of body weight. In addition to modulating feeding behavior, the brain is involved in the control of energy expenditure through regulation of basal metabolism, adaptive thermogenesis, and locomotor activity. In this regard, a hypothalamic network including the arcuate nucleus, ventromedial and lateral hypothalamus, and paraventricular nucleus (PVN) is crucial for regulating feeding behavior and thermogenesis (1–3).

Several studies have implicated the PVN in the autonomic control of energy expenditure by modulating sympathetic outflow to brown adipose tissue (BAT) (4, 5). BAT transforms energy from substrates into heat by free fatty acid oxidation (6), a crucial function for thermoregulation during cold stress and regulation of body weight. Alterations in BAT function may be involved in diet-induced obesity (DIO) (7). Previous reports suggested that a population of neurons within the PVN activate BAT thermogenesis via the sympathetic nervous system (4). In contrast, a more recent study suggests that PVN neurons send signals to reduce BAT sympathetic nerve activity (8). Thus, while the involvement of the PVN in regulating BAT activity has been demonstrated, it remains unclear whether alterations in PVN control of BAT activity contribute to DIO.

White adipose tissue (WAT) is metabolically less active than BAT and is specialized for storing chemical energy. Sympathetic stimulation of WAT induces breakdown of triacylglycerol via hormone-sensitive lipase (9). Recent studies show that increased norepinephrine in WAT induces expression of uncoupling protein 1 (*Ucp1*) and increases metabolic activity (10). The increased *Ucp1* expression in WAT is termed browning (10). Importantly, browning of WAT has antiobesity effects (11, 12), and the PVN is involved in regulating sympathetic outflow to WAT (13, 14). Furthermore, bilateral lesioning of the PVN reduces sympathetic signaling and diminishes lipid mobilization (15). The involvement of the PVN in browning

Authorshop notes: H.E Lob and J. Song contributed equally to this work. A.L. Mark and R.L. Davisson are co-senior authors.

Conflict of interest: The authors have declared that no conflicts of interest exist.

Submitted: February 15, 2016
Accepted: December 13, 2016
Published: January 26, 2017

Reference information:
JCI Insight. 2017;2(2):e87094.
doi:10.1172/jci.insight.87094.

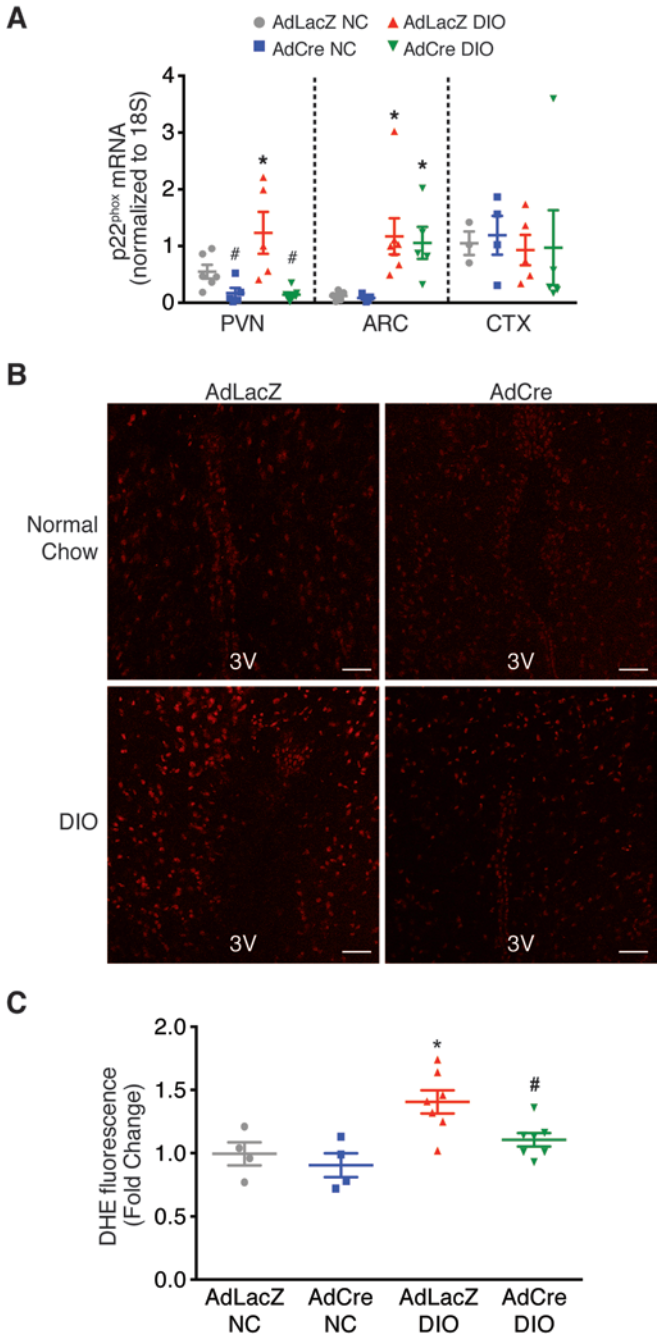

Figure 1. AdCre targeted to the PVN of *p22*$^{phox/fl}$ mice is effective and selective in blunting *p22*^{phox} mRNA and DIO-induced production of ROS in this hypothalamic region. (**A**) Effects of periventricular nucleus–targeted (PVN-targeted) AdCre or AdLacZ on *p22*^{phox} expression in the PVN, arcuate nucleus (ARC), and cerebral cortex (CTX) in normal chow–fed (NC-fed) and diet-induced obesity (DIO) *p22*$^{phox/fl}$ mice. **P* < 0.05 vs. NC; #*P* < 0.05 AdCre vs. AdLacZ; *n* = 5–6. (**B**) Representative images of dihydroethidium (DHE) fluorescence in the PVN of *p22*$^{phox/fl}$ mice that were microinjected with AdLacZ (left panels) or AdCre (right panels) and received 10 weeks NC (upper panels) or high-fat diet (lower panels). Scale bars: 100 μm. (**C**) Mean DHE fluorescence intensity. **P* < 0.05 vs. NC; #*P* < 0.05 AdCre DIO vs. AdLacZ DIO; *n* = 4–7. All data are the mean ± SEM. All *P* values determined by 1-way ANOVA followed by Tukey's post-hoc test.

has yet to be determined. Collectively, these findings demonstrate a role of the PVN in energy homeostasis and suggest that changes in this brain region might influence adiposity and obesity.

Chronic oxidative stress contributes to pathophysiological conditions such as atherosclerosis and hypertension (16, 17). Further, excess generation of reactive oxygen species (ROS) is an underlying mechanism of metabolic disorders (18), and oxidative stress in adipose tissue has a central role in the pathogenesis of metabolic syndrome and type 2 diabetes (19). Chronic overnutrition contributes to hypothalamic inflammation and endoplasmic reticulum (ER) stress, both of which are linked to oxidative stress (20–22). NADPH oxidases are major sources of ROS in a variety of chronic diseases such as hypertension (23). The catalytic subunits of NADPH oxidases are Nox proteins (Nox1, Nox2 [gp91^{phox}], Nox3, and Nox4), which, in rodents, require the membrane protein p22^{phox} to be active (17). Thus, alterations in *p22*^{phox} regulate cellular NADPH oxidase activity and ROS production (23–25). Interestingly, a recent study linked vascular *p22*^{phox}-mediated oxidative stress to accelerated weight gain during high-fat diet (HFD) (26).

While these and other investigations have focused on oxidative stress in peripheral tissues during obesity, recent evidence has suggested that NADPH oxidase–dependent oxidative stress in the CNS is involved in the regulation of body weight and adipose tissue metabolism (22). A recent study showed that DIO increased hypothalamic expression of NADPH oxidase, a major source of ROS (27). However, a causal link between increased hypothalamic NADPH oxidase and obesity has not been investigated.

We provide evidence that deletion of *p22*^{phox} and inhibition of NADPH oxidase–derived oxidative stress selectively in the PVN increases BAT thermogenesis and browning of subcutaneous WAT via a β_3-adrenoceptor–dependent pathway during DIO. This results in increased energy expenditure and less adiposity and weight gain during HFD, independent of changes in food intake or locomotor activity. Our findings establish a causal link between oxidative stress in the PVN and obesity, and advance our understanding of the neural regions and metabolic mechanisms involved.

Results

Selective deletion of p22^{phox} *in the PVN blunts ROS production during DIO.* AdCre was injected bilaterally into the PVN of *p22*$^{phox/fl}$ mice to eliminate this critical NADPH oxidase subunit selectively from the PVN. Control *p22*$^{phox/fl}$ animals were injected with AdLacZ. Following 7–10 days of recovery, mice were fed HFD or remained on normal chow (NC) for 10 weeks. At the end of this period, we verified that AdCre reduced *p22*^{phox} expression in the PVN. Quantitative real-time PCR from micropunches of the PVN showed

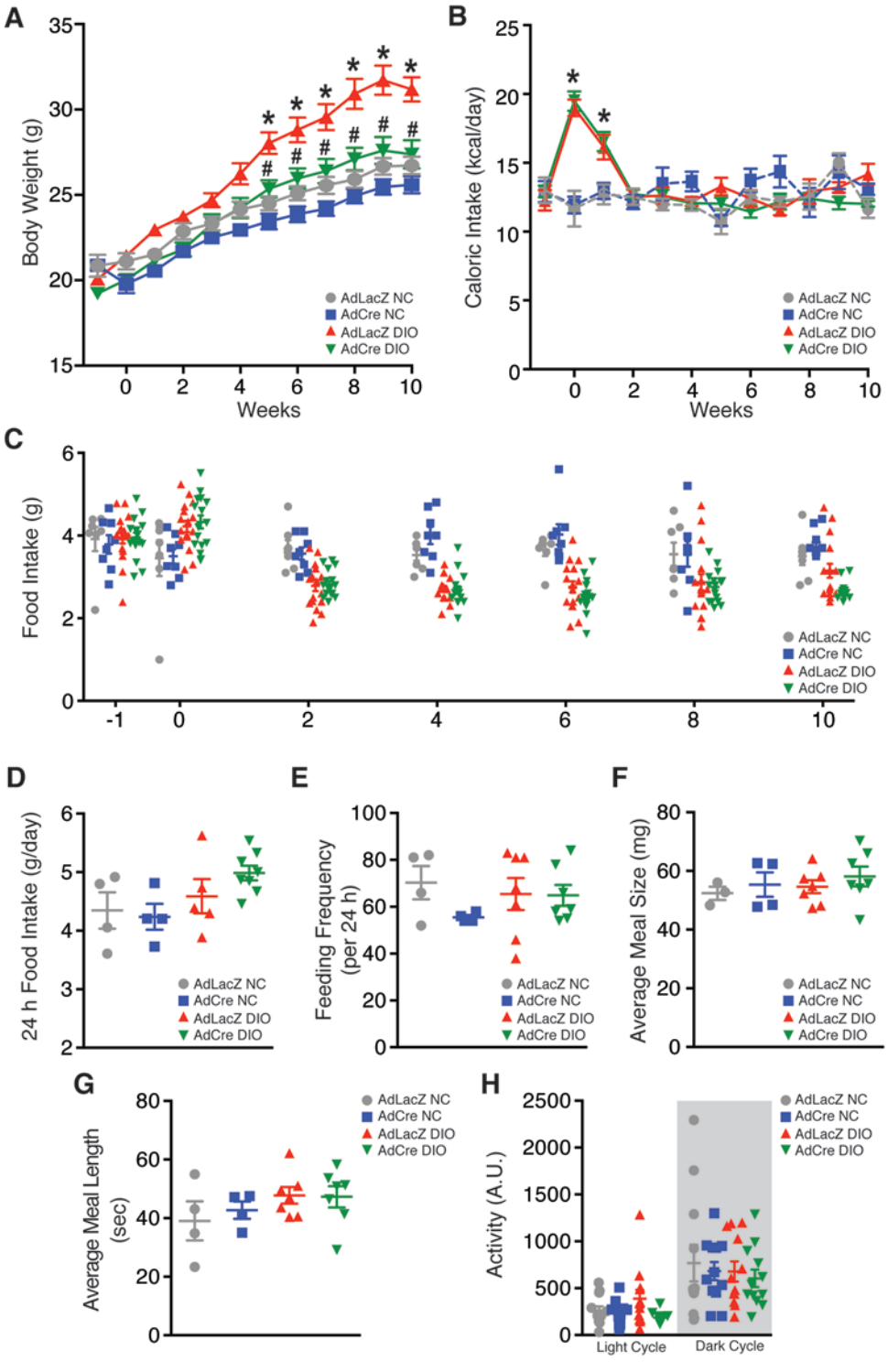

Figure 2. Ablation of *p22*^{phox} in the periventricular nucleus ameliorates body weight gain independent of food intake, eating behavior, and activity. (**A** and **B**) Body weight gain (**A**, *n* = 13–19) and caloric intake (**B**, *n* = 8–17) in AdLacZ- or AdCre-treated *p22*$^{phox/fl}$ mice during 10 weeks of normal chow (NC) or diet-induced obesity (DIO). (**C**) Weekly food intake in AdLacZ or AdCre mice during 10 weeks of NC or DIO (*n* = 7–17). (**D**–**G**) Food intake (**D**), feeding frequency (**E**), average meal size (**F**), and average meal length (**G**) measured by indirect calorimetry in AdLacZ- or AdCre-injected *p22*$^{phox/fl}$ mice over 24 hours (*n* = 4–8). (**H**) Spontaneous locomotor activity during the light and dark cycles in AdLacZ and AdCre mice after 10 weeks of NC or high-fat diet (*n* = 4–8). The gray area indicates the dark cycle between 6 pm and 6 am.*$P < 0.05$ vs. NC; $^{\#}P < 0.05$ vs. AdLacZ DIO; 2-way ANOVA followed by a Sidak multiple comparison post-hoc test. All data are the mean ± SEM.

that whereas DIO increased PVN *p22*^{phox} mRNA expression in control vector–treated animals, targeting of AdCre to this brain area prevented the HFD-induced increase in *p22*^{phox} in the PVN (Figure 1A). We found no change in *p22*^{phox} expression in the arcuate nucleus or cerebral cortex (CTX) after AdCre injection in the PVN, demonstrating the selectivity of AdCre for the PVN (Figure 1A).

To verify that deletion of *p22*^{phox} in the PVN leads to functional inactivation of NADPH oxidase, ROS were measured with dihydroethidium (DHE) staining (Figure 1, B and C). Ten weeks of HFD resulted in a significant increase in DHE fluorescence in the PVN (Figure 1, B and C). AdCre injection into the PVN blunted the increase in DHE fluorescence during HFD (Figure 1, B and C). During NC, AdCre injection did not alter DHE fluorescence in the PVN (Figure 1, B and C).

Deletion of p22^{phox} *protects against weight gain in DIO mice*. Next, we studied the physiological effects of *p22*^{phox} deletion in the PVN during DIO in AdLacZ- or AdCre-injected *p22*$^{phox/fl}$ mice. Removal of *p22*^{phox} from the PVN abolished the body weight gain in response to HFD compared with mice treated with AdLacZ (Figure 2A). Injection of AdCre in the PVN did not alter body weight in mice fed NC (Figure 2A). Food intake increased transiently during HFD but did not differ between mice with PVN injection of AdLacZ versus AdCre (Figure 1B). Importantly, prevention of weight gain in AdCre mice was not accounted for by differences in caloric or food intake between AdLacZ- and AdCre-injected mice (Figure 2, B and C).

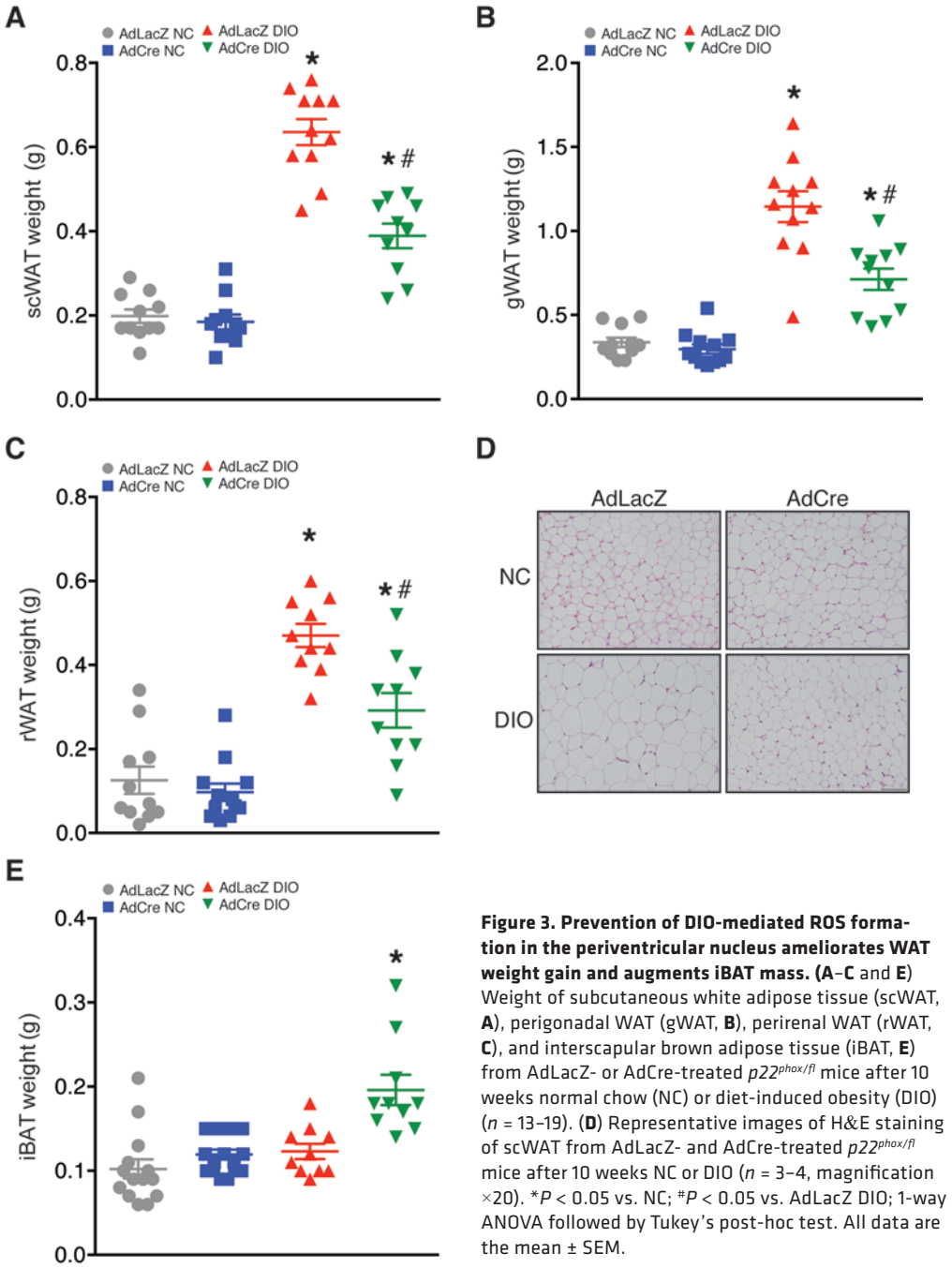

Figure 3. Prevention of DIO-mediated ROS formation in the periventricular nucleus ameliorates WAT weight gain and augments iBAT mass. (A–C and **E)** Weight of subcutaneous white adipose tissue (scWAT, **A**), perigonadal WAT (gWAT, **B**), perirenal WAT (rWAT, **C**), and interscapular brown adipose tissue (iBAT, **E**) from AdLacZ- or AdCre-treated $p22^{phox/fl}$ mice after 10 weeks normal chow (NC) or diet-induced obesity (DIO) (n = 13–19). (**D**) Representative images of H&E staining of scWAT from AdLacZ- and AdCre-treated $p22^{phox/fl}$ mice after 10 weeks NC or DIO (n = 3–4, magnification ×20). $^{*}P < 0.05$ vs. NC; $^{\#}P < 0.05$ vs. AdLacZ DIO; 1-way ANOVA followed by Tukey's post-hoc test. All data are the mean ± SEM.

Food intake monitored during indirect calorimetry at the end of the 10-week period also demonstrated that selective ablation of $p22^{phox}$ from the PVN did not influence food intake, feeding frequency, average meal size or meal length (Figure 2, D–G). Together, these findings demonstrate that the observed effect of ablation of $p22^{phox}$ in the PVN on body weight in DIO mice is independent of food and caloric intake.

We also tested the possibility that the prevention of weight gain during DIO was due to increased locomotor activity. Spontaneous locomotor activity as measured by laser beam breaks in an indirect calorimetry system did not differ between AdLacZ and AdCre PVN-targeted animals during either the light or dark cycles (Figure 2H). Thus, the blunting of weight gain in AdCre-treated $p22^{phox/fl}$ mice was also independent of locomotor activity.

$p22^{phox}$ deletion in the PVN blunts WAT accumulation and augments iBAT during DIO. Given the finding that ablation of $p22^{phox}$ from the PVN prevented HFD-induced increases in body weight (Figure 2A), we also examined regional adipose tissue depots following HFD and NC feeding. As expected, AdLacZ-treated

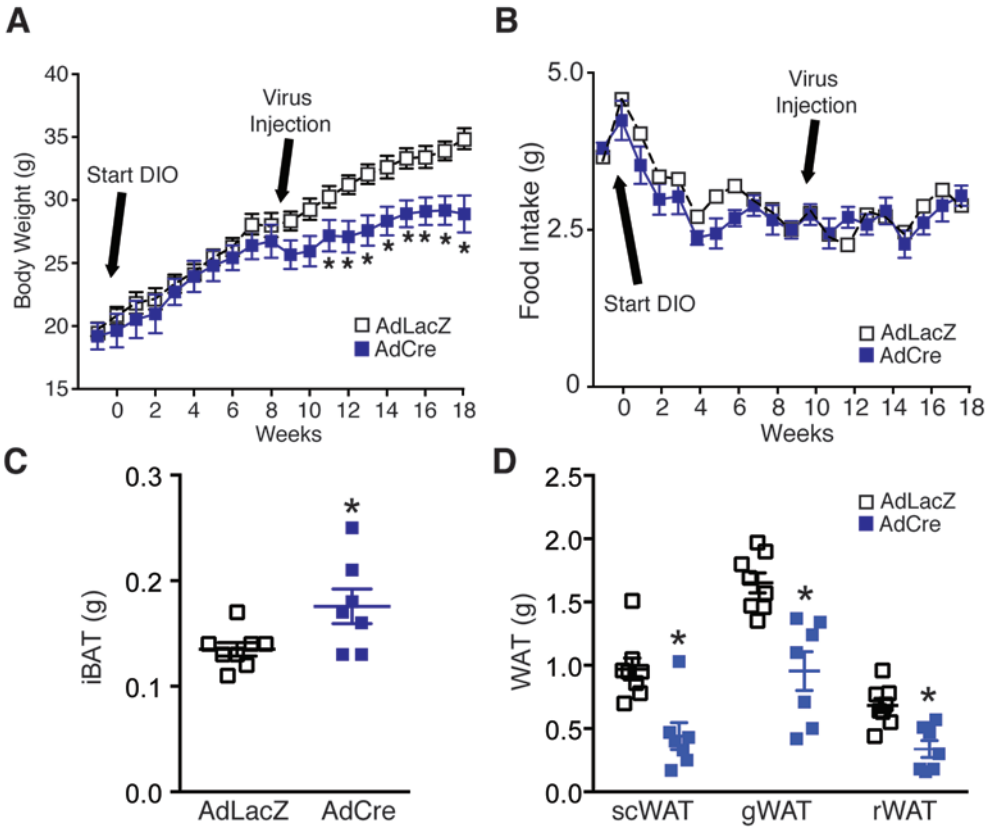

Figure 4. Reduction in *p22*^{phox} in the periventricular nucleus (PVN) arrests further weight gain in obese animals. (**A**) Effects of PVN *p22*^{phox} deletion on body weight in mice fed high-fat diet for 8 weeks prior to and 10 weeks after injection of AdLacZ or AdCre in *p22*$^{phox/fl}$ mice. (**B**) Average food intake before and after viral transfection in these mice. (**C** and **D**) Interscapular brown adipose tissue (iBAT) and white adipose tissue (WAT) weights taken at the termination of the experiments from the above animals (sc, subcutaneous; g, gonadal; r, renal). *$P < 0.05$ AdCre vs. AdLacZ, $n = 7–8$; 2-way ANOVA followed by a Sidak multiple comparison post-hoc test (**A** and **B**), 1-way ANOVA followed by Tukey's post-hoc test (**C** and **D**). All data are the mean ± SEM.

DIO mice exhibited significant increases in various WAT masses, including subcutaneous (sc), perigonadal (g), and perirenal (r) WAT after 10 weeks of HFD (Figure 3, A–C). Deletion of *p22*^{phox} in the PVN caused a significant attenuation in HFD-induced increases in mass of these WAT depots (Figure 3, A–C). As seen in representative histological images of scWAT in Figure 3D, adipocytes were enlarged after 10 weeks of HFD in control vector–treated mice. In HFD-fed mice lacking *p22*^{phox} in the PVN, cells were similar in size to those of NC-fed controls.

Since BAT is the major site of adaptive thermogenesis and is thus crucial in body weight regulation (6), we also measured interscapular BAT (iBAT) mass. AdLacZ-treated *p22*$^{phox/fl}$ mice showed no change in iBAT mass after 10 weeks of HFD, whereas iBAT mass was significantly increased in DIO mice with targeted ablation of *p22*^{phox} in the PVN (Figure 3E). Neither iBAT nor WAT weights were altered by AdCre in NC-fed mice (Figure 3, A–C, E).

After the onset of obesity, p22^{phox} *ablation in the PVN blunts further increases in adiposity and body weight gain*. To determine if HFD-induced weight gain and adiposity could be arrested by removal of *p22*^{phox} from the PVN after the onset of obesity, a separate cohort of *p22*$^{phox/fl}$ mice was fed HFD for 8 weeks to induce obesity prior to targeting the PVN with AdCre or AdLacZ. The mice in the 2 groups gained a similar amount of body weight during the first 8 weeks of HFD (Figure 4A). However, as body weight continued to increase in AdLacZ mice, AdCre-treated mice showed no further weight gain compared with AdLacZ mice over the next 10 weeks of HFD feeding (Figure 4A). This was independent of changes in food intake (Figure 4B). Corresponding to body weight, in mice with PVN injections of AdCre or AdLacZ after 8 weeks of HFD, WAT mass was lower and iBAT mass higher in the AdCre mice after 18 weeks of HFD (Figure 4, C and D).

p22^{phox} *in the PVN is involved in the regulation of energy expenditure during the development of DIO*. Next we investigated the underlying mechanism(s) of the beneficial effects of PVN *p22*^{phox} deletion on body weight and adiposity during HFD by measuring oxygen consumption (VO_2) and heat production using indirect calorimetry at the end of the 10-week protocol. As expected for nocturnal animals, VO_2 and heat production were higher during the dark cycle (Figure 5, A and B). AdCre-targeted PVN injections did not alter VO_2 or heat production in mice fed NC (Figure 5, A and B). In addition, HFD had no effect on these parameters in AdLacZ-treated mice. However, targeted deletion of *p22*^{phox} in the PVN caused a significant

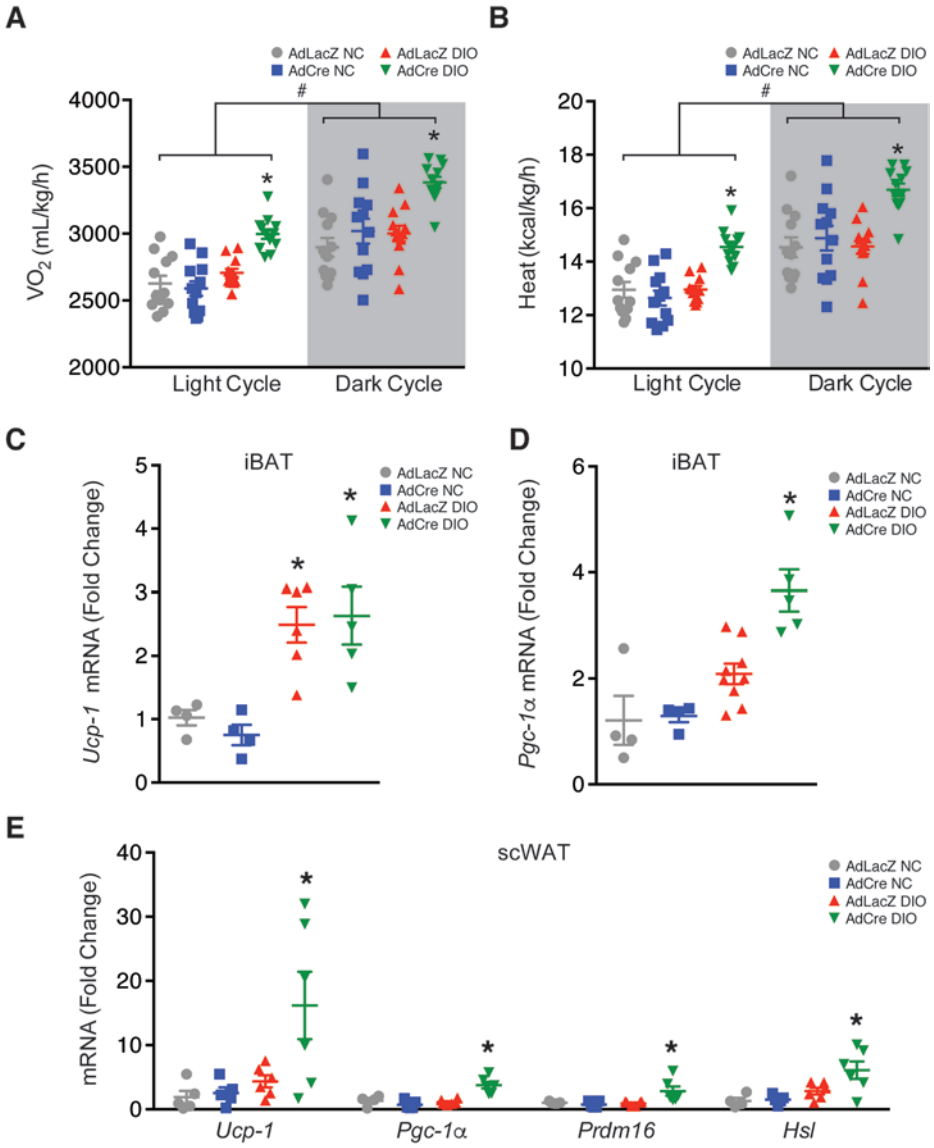

Figure 5. *p22*^{phox} deletion in the PVN elevates thermogenesis and promotes increased expression of Ucp-1 and Pgc-1α in iBAT and browning of scWAT. (**A**) Average oxygen consumption (VO_2) and (**B**) heat production in AdLacZ- and AdCre-treated *p22*$^{phox/fl}$ mice after 10 weeks normal chow (NC) or diet-induced obesity (DIO). **P* < 0.05 vs. NC and AdLacZ DIO; #*P* < 0.05 Dark vs. Light Cycle; *n* = 4–8. Gray area indicates dark cycle between 6 pm and 6 am. (**C**) *Ucp-1* mRNA expression in interscapular brown adipose tissue (iBAT). **P* < 0.05 vs. NC, *n* = 10–16. (**D**) Expression of thermogenic marker *Pgc-1α* in iBAT (*n* = 10–16). **P* < 0.05 vs. NC and AdLacZ DIO; #*P* < 0.05 vs. NC. (**E**) Expression of *Ucp-1*, *Pgc-1α*, *Prdm16*, and *Hsl* mRNA in subcutaneous white adipose tissue (scWAT) in AdLacZ and AdCre mice after 10 weeks NC or high-fat diet (*n* = 11). **P* < 0.05 vs. NC and AdLacZ DIO. All data are the mean ± SEM. All *P* values determined by 1-way ANOVA followed by Tukey's post-hoc test.

increase in VO_2 and heat production throughout a 24-hour period (both light and dark cycles) during DIO (Figure 5, A and B). This indicates that prevention of HFD-induced increases in NADPH oxidase–dependent ROS production in the PVN elevates energy expenditure and thermogenesis.

p22^{phox} *deletion in the PVN increased Ucp-1 mRNA and peroxisome proliferator-activated receptor gamma coactivator 1-alpha mRNA (Pcg-1α) in iBAT during DIO.* Given the increased iBAT mass along with elevated VO_2 and heat production in HFD-fed mice following selective removal of *p22*^{phox} from the PVN, we investigated expression of adaptive thermogenesis markers in iBAT including *Ucp-1* and *Pgc-1α*. Consistent with previous findings (28, 29), iBAT *Ucp-1* mRNA was increased ~3-fold after 10 weeks of DIO in AdLacZ-injected *p22*$^{phox/fl}$ mice (Figure 5C). Deletion of *p22*^{phox} in the PVN did not result in a further increase in iBAT *Ucp-1* mRNA compared with AdLacZ DIO mice (Figure 5C). In contrast, *Pgc-1α* mRNA expression was increased ~4-fold in iBAT after deletion of *p22*^{phox} in the PVN during DIO (Figure 5D). *Pgc-1α* expression was not significantly increased in AdLacZ DIO mice (Figure 5D), nor was it increased in NC mice.

Deletion of p22^{phox} *in the PVN during DIO induces browning in scWAT.* A recent study showed that activation of the hypothalamic-adipocyte axis promotes a phenotypic switch of scWAT to a brown-like adipose tissue (30). Since deletion of *p22*^{phox} in the PVN was associated with a significant reduction in WAT in the face of HFD (Figure 3, A–C), we speculated that browning and lipolysis of WAT may be involved (9). Markers of WAT browning including *Ucp-1*, *Pgc-1α*, and PR-domain-containing 16 (*Prdm16)* (30–32) were evaluated in scWAT. There was no significant increase in scWAT *Ucp-1*, *Pgc-1α*, or *Prdm16* mRNA expression in DIO mice with PVN injection of AdLacZ (Figure 5E). In contrast, deletion of PVN *p22*^{phox} in DIO mice caused a striking increase in scWAT *Ucp-1* (~20-fold), *Pgc-1α* (~4-fold), and *Prdm16* (~3-fold) mRNA expression (Figure 5E). None of these markers was altered in NC-fed mice. We also measured mRNA expression of hormone-sensitive lipase (*Hsl*), an enzyme necessary to promote lipolysis in WAT (33). HFD did not increase expression of *Hsl* in AdLacZ-treated mice, whereas AdCre-treated mice showed an ~6-fold

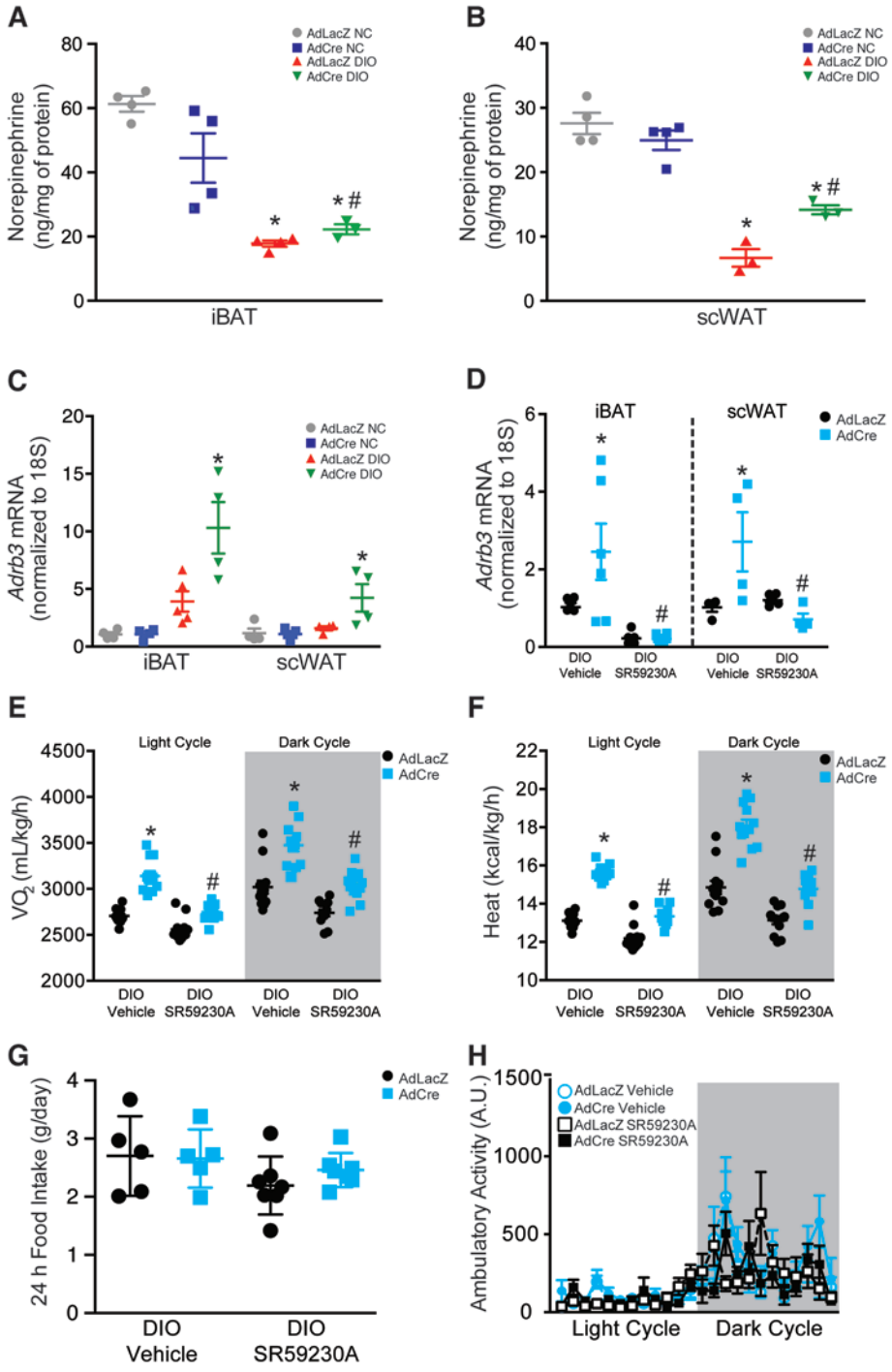

Figure 6. Increased energy expenditure after *p22^{phox}* deletion in the periventricular nucleus is due to *Adrb3*-mediated mechanisms. (**A** and **B**) Norepinephrine levels in interscapular brown adipose tissue (iBAT) and subcutaneous white adipose tissue (scWAT) of AdLacZ- and AdCre-treated *p22$^{phox/fl}$* mice after 10 weeks of high-fat diet (HFD) or normal chow (NC). **P* < 0.05 vs. NC; $^{\#}$*P* < 0.05 AdCre diet-induced obesity (DIO) vs. AdLacZ DIO; *n* = 3–4. (**C**) *Adrb3* mRNA expression in iBAT and scWAT in AdLacZ- and AdCre-treated mice after 10 weeks of NC or HFD. **P* < 0.05 vs. NC and AdLacZ DIO; *n* = 4–6. (**D**–**H**) Effect of SR59230A (i.p.) on *Adrb3* in iBAT and scWAT (**D**), oxygen consumption (VO_2) (**E**), heat production (**F**), food intake (**G**), and spontaneous locomotor activity (**H**) in AdLacZ or AdCre DIO animals during 3 days of SR59230A injections (*n* = 5–6). **P* < 0.05 AdCre DIO vehicle vs. AdLacZ DIO vehicle; $^{\#}$*P* < 0.05 AdCre DIO SR59230A vs. AdCre DIO vehicle. The gray area indicates the dark cycle between 6 pm and 6 am. All data are the mean ± SEM. All *P* values determined by 1-way ANOVA followed by Tukey's post-hoc test.

increase in *Hsl* mRNA (Figure 5E). As above, mice fed NC did not show changes in *Hsl* transcript levels.

Ablation of p22^{phox} in the PVN attenuates increased adiposity during HFD by activation of β_3-adrenoceptors in iBAT and scWAT. Previous studies implicate sympathetic signals from the PVN in the regulation of thermogenesis by stimulating BAT and WAT activity (5, 13, 15, 34). Thus, we investigated if deletion of PVN *p22^{phox}* alters norepinephrine (NE) levels in iBAT and scWAT.

NE levels in iBAT and scWAT were lower in mice fed HFD than in mice fed NC (Figure 6, A and B). Deletion of *p22^{phox}* in the PVN of NC-fed mice did not significantly alter NE in iBAT or scWAT (Figure 6, A and B). In contrast, deletion of *p22^{phox}* in the PVN increased NE levels in both iBAT and scWAT after 10 weeks of DIO, suggesting that PVN ROS inhibits NE levels in adipose depots during HFD (Figure 6, A and B) (35).

Given the prominent role of β_3-adrenoceptors (*Adrb3*) in thermogenic and lipolytic processes in both BAT and WAT (5, 6, 13, 34), we next examined expression of *Adrb3* in iBAT and scWAT. AdCre injections did not change *Adrb3* expression in *p22$^{phox/fl}$* mice fed NC compared with AdLacZ control mice (Figure 6C). Further, DIO did not significantly increase *Adrb3* mRNA in iBAT or scWAT in AdLacZ DIO mice (Figure 6C). In contrast, deletion of *p22^{phox}* in the PVN of AdCre-treated mice led to striking increases in *Adrb3* mRNA in both iBAT (~10-fold vs. AdLacZ NC) and scWAT (~4-fold vs. AdLacZ NC) during HFD (Figure 6C).

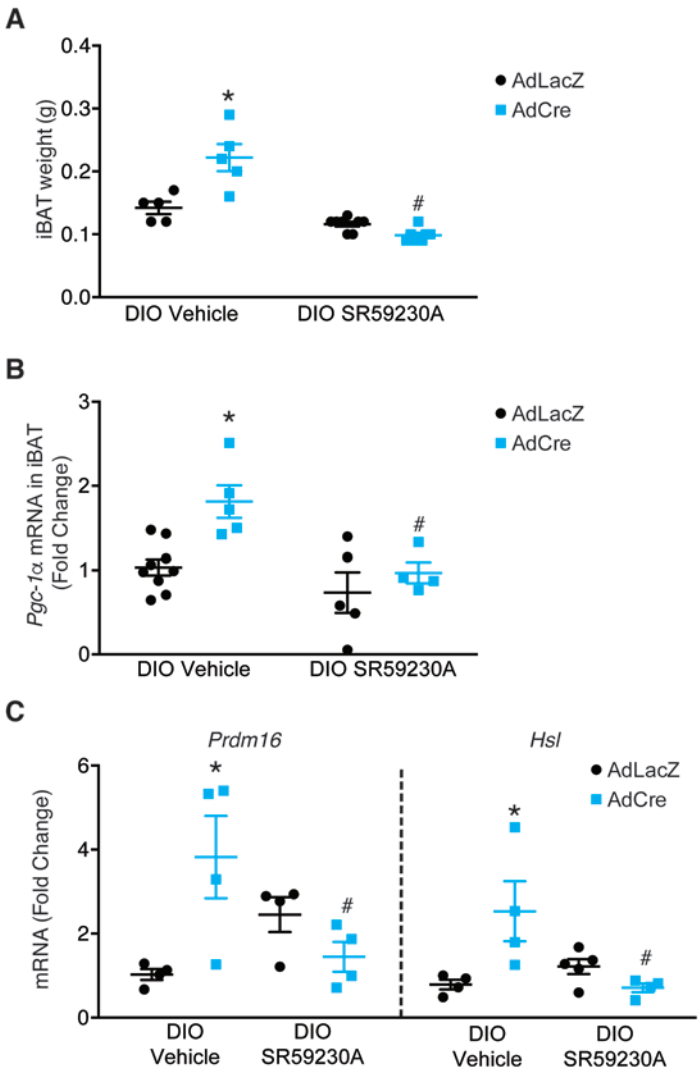

Figure 7. Blockade of β_3-adrenoceptors decreases iBAT mass and *Pcg-1α*, and thermogenic markers in scWAT. Effect of SR59230A (i.p.) on interscapular brown adipose tissue (iBAT) weight (**A**), iBAT *Pgc-1α* mRNA (**B**), and thermogenic markers (*Prdm16* and *Hsl*) in subcutaneous white adipose tissue (scWAT, **C**) in AdLacZ- and AdCre-treated $p22^{phox/fl}$ mice after 10 weeks of normal chow (NC) or diet-induced obesity (DIO) (n = 4–9). $^*P < 0.05$ AdCre DIO vehicle vs. AdLacZ DIO vehicle; $^{\#}P < 0.05$ AdCre DIO SR59230A vs. AdCre DIO vehicle; 1-way ANOVA followed by Tukey's post-hoc test. All data are the mean ± SEM.

To investigate the functional role of an upregulation of β_3-adrenoceptors in DIO mice lacking $p22^{phox}$ we injected (i.p.) animals daily with SR59230A, a selective β_3-adrenoceptor antagonist (36). Relative to vehicle-injected AdCre DIO mice, SR59230A significantly reduced *Adrb3* mRNA in iBAT and scWAT of AdCre-treated DIO mice (Figure 6D). Blockade of β_3-adrenoceptors also decreased VO_2 and heat production in AdCre DIO mice compared with AdCre vehicle controls (Figure 6, E and F). The reductions in VO_2 and heat production were independent of alterations in food intake or locomotor activity (Figure 6, G and H). Furthermore, SR59230A caused a significant reduction in iBAT mass (>50%) and *Pgc-1α* mRNA in DIO mice lacking $p22^{phox}$. β_3-Adrenoceptor blockade did not alter iBAT mass or *Pgc-1α* mRNA in DIO without deletion of PVN $p22^{phox}$ (Figure 7, A and B), suggesting that β_3-adrenoceptor–mediated mechanisms contribute to the increased iBAT mass and augmented *Pgc-1α* levels in DIO mice with deletion of PVN $p22^{phox}$. Blockade of the β_3-adrenoceptors also ameliorated scWAT *Prdm16* and *Hsl* expression in DIO mice with deletion of PVN $p22^{phox}$, indicating reduced browning and lipolysis of scWAT (Figure 7C). Blockade of β_3-adrenoceptors did not affect these variables in AdLacZ DIO mice (Figure 7C).

Discussion

This study reveals a potentially novel role for NADPH oxidase–derived ROS in the PVN in the regulation of metabolic homeostasis and HFD-induced obesity. Selective deletion of $p22^{phox}$ in this brain region increases thermogenesis and BAT mass and induces browning and decreases of scWAT by β_3-adrenergic–mediated mechanisms. This is accompanied by attenuation of WAT mass and body weight during HFD. Notably, these effects are independent of changes in caloric intake or locomotor activity.

Links between brain NADPH oxidase–derived ROS and cardiovascular disease are well established (23) and are emerging in DIO (22, 27). The subunit $p22^{phox}$ is not catalytically active, but is critical for proper functioning of all rodent NADPH oxidase isoforms (37). Increased expression of $p22^{phox}$ is an indicator of increased NADPH oxidase activity (23, 38), and elevated $p22^{phox}$ in the vasculature was recently linked to accelerated obesity during HFD (26). Here we observed HFD-induced elevations in $p22^{phox}$ expression and corresponding increases in ROS as indicated by DHE fluorescence in the PVN, both of which were abolished by viral gene transfer of Cre recombinase selectively to this brain region. Tissue samples for these studies were obtained 11 weeks after gene transfer, indicating that AdCre induced a highly stable reduction in $p22^{phox}$ in this region throughout the course of the experiments. This is consistent with previous studies using a similar approach in different brain sites (23). Importantly, PVN-targeted AdCre did not alter $p22^{phox}$ expression in another important metabolic center of the brain, the arcuate nucleus or in the CTX, indicating the site selectivity of PVN deletion of $p22^{phox}$.

The protective effects of $p22^{phox}$ deletion on weight gain and adiposity during DIO were independent of energy intake and locomotor activity. We also did not observe differences in other feeding parameters

including the frequency of feeding, average meal size, or length of time spent feeding. Interestingly, caloric intake was only elevated in the first week of HFD. This finding is in agreement with previous studies showing that HFD-fed mice and rats have, after an initial elevation in caloric intake, similar caloric intake compared with NC-fed animals (26, 39). Similar observations have been made in primates (40). These findings suggest that rodents and primates adapt quickly to the increased nutrient availability and increased caloric intake is not sustained over a long period of time. The exact mechanisms of this caloric adaption remain elusive. However, NADPH oxidase–dependent oxidative stress in the PVN does not seem to play a role in the calorie adaption in our study since there was no difference in food intake between HFD DIO mice with or without deletion of PVN *p22^{phox}*.

Next we tested if removal of *p22^{phox}* can halt progression of DIO. For this we fed the animals HFD before transfection with adenoviral vectors. Our results show that further weight gain in obese animals was arrested upon deletion of *p22^{phox}* in the PVN despite continued HFD feeding. This effect on weight gain was again independent of changes in caloric intake. These studies indicate that deletion of *p22^{phox}* in the PVN not only prevents lean animals from becoming obese during HFD, but also slows further weight gain in obese animals.

Previous studies have implicated the PVN in control of sympathetic outflow to BAT (4, 5), and thereby the regulation of thermogenesis and energy expenditure (6). Here we determined that HFD-fed animals lacking PVN *p22^{phox}* exhibited increased iBAT mass and elevated energy expenditure and thermogenesis. We pursued this by investigating the expression of the adaptive thermogenesis markers *Ucp-1* and *Pgc-1α* in iBAT. UCP-1 uncouples the respiratory chain in mitochondria and creates heat, and *Pgc-1α* is a coactivator gene required for brown fat thermogenesis (32). We confirmed previous findings that *Ucp-1* mRNA is elevated in response to HFD in control mice (28, 29), but *Ucp-1* mRNA did not increase further with deletion of PVN *p22^{phox}*. We cannot explain this finding, but note that *Pgc-1α* mRNA in iBAT was elevated in AdLacZ DIO mice and increased further in AdCre DIO mice lacking PVN *p22^{phox}*. Thus, despite the unexplained failure of iBAT *Ucp-1* mRNA to increase with deletion of PVN *p22^{phox}*, we suggest that the data on *Pgc-1α* mRNA in iBAT support our conclusion that deletion of PVN *p22^{phox}* augments thermogenesis in iBAT.

Recent findings indicate that a phenotypic switch of WAT to a brown-like adipose tissue contributes to thermogenesis (12, 30). Given that the PVN is involved in the sympathetic regulation of WAT (13, 14), we investigated if deletion of *p22^{phox}* in this brain region induces browning of WAT. Increased expression of *Prdm16*, *Ucp-1*, and *Pgc-1α* in WAT correlates with the metabolic activity of these tissues, which is referred to as browning of white fat (11, 31, 32). We focused on scWAT, because it is especially prone to browning (11). Deletion of *p22^{phox}* in the PVN of DIO mice was associated with increased expression of each of these browning markers in scWAT. Browning of WAT was also associated with elevated lipolysis as indicated by augmented *Hsl* expression (41). Indeed, DIO mice with targeted deletions of *p22^{phox}* in the PVN showed increased *Hsl* mRNA in scWAT. These data suggest that a reduction in NADPH oxidase–dependent oxidative stress in the PVN elevates metabolic activity in scWAT during DIO. This contributes to the observed attenuation of WAT mass and increased thermogenesis.

Deletion of *p22^{phox}* in the PVN augmented β_3-adrenoceptor expression in iBAT and scWAT during DIO, and this was prevented by selective β_3-adrenoceptor blockade with SR59230A. This suggests that blunting of oxidative stress in the PVN during DIO leads to increased β_3-adrenoceptor activity that contributes to increased energy expenditure in both iBAT and scWAT (32). A recent study showed that NE stimulates blood flow to iBAT (42).

PVN-derived sympathetic signals are involved in the regulation of thermogenesis by stimulating BAT and WAT metabolism (5, 15). Adipose NE levels were higher in mice fed NC than in DIO mice and were not altered by deletion of *p22^{phox}* in the PVN, suggesting that PVN ROS was not appreciably limiting adipose NE in mice fed NC. In contrast, deletion of PVN *p22^{phox}* in DIO mice increased adipose NE levels, particularly in scWAT. These data suggest that PVN ROS modulate scWAT NE levels in DIO mice but not in mice fed NC. This may indicate that the increase in energy expenditure with deletion of PVN *p22^{phox}* may be due primarily to elevated metabolic activity of the scWAT. Although an indirect indicator of sympathetic activity, the adipose NE levels taken together with the increased *Adrb3* expression in iBAT and scWAT of AdCre DIO mice suggest that PVN ROS modulate adipose NE levels in DIO mice but not in mice fed NC. Increased oxidative stress in certain brain regions, including the PVN, has been shown to increase sympathetic nerve activity (43–45). In contrast, our data suggest that in DIO mice, blunting of oxidative stress in the PVN contributes to elevated sympathetic activity in adipose tissue regions. Recent evidence shows that some neurons in the

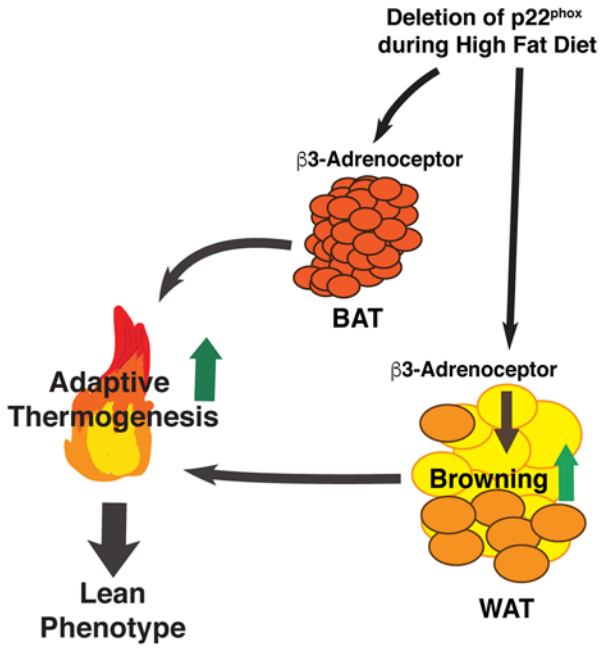

Figure 8. Schematic of proposed mechanisms. Selective deletion of *p22*^{phox} and a reduction in *p22*^{phox}-derived ROS in the periventricular nucleus during high-fat diet (HFD) feeding activates β_3-adrenoceptor–dependent pathways to increase adaptive thermogenesis and blunting of weight gain during HFD. BAT, brown adipose tissue; WAT, white adipose tissue.

PVN inhibit sympathetic outflow (8). We speculate that deletion of *p22*^{phox} and reduction of ROS in the PVN may increase sympathetic outflow to adipose tissues by reducing inhibitory signals. In support of this concept are recent findings that scavenging ROS increased the excitability of spinal GABA neurons in mice (46).

A recent study in human subjects showed that β_3-adrenoceptor–mediated mechanisms elevate resting metabolic rate and activate BAT and WAT metabolism (47). Our findings that SR59230A attenuated *Adrb3* mRNA in BAT and scWAT, blunted the increased VO_2 and heat production, and reduced scWAT browning in AdCre-treated DIO mice are consistent with the conclusion that β_3-adrenergic mechanisms are at play in the increased thermogenesis and energy expenditure observed in DIO mice lacking *p22*^{phox} in our study. It should be noted that SR59230A crosses the blood brain barrier and acts on CNS β_3-adrenoceptors (48, 49). Thus, the possibility of the involvement of CNS β_3-adrenoceptor–dependent mechanisms following SR59230A injection cannot be excluded. However, given that β_3-adrenoceptors are expressed in the rodent hypothalamus at very low levels (50), it is likely that peripheral adipose tissue β_3-adrenoceptor–dependent mechanisms are primarily responsible for the observations in our study.

Although we and others have demonstrated the importance of sympathetic signaling in adipose tissue (5, 13, 34), we recognize the potential importance of oxidative stress in the PVN in the regulation of the hypothalamic-pituitary-adrenal and hypothalamic-pituitary-thyroid axes during HFD. The PVN plays a major role in the activity of both of these hormonal systems (51–53). Obesity alters the activity of both hormonal systems (54, 55). High-fat feeding per se increases the activity of the hypothalamic-pituitary-adrenal axis (56). Chronic elevation of glucocorticoids contributes to obesity (57). DIO furthermore increases circulating thyroid hormones (58). The role of oxidative stress during obesity in the activation of these hormonal systems remains undefined.

Our data demonstrate that selective reduction in *p22*^{phox}-derived ROS in the PVN during HFD feeding increases iBAT thermogenesis and browning of scWAT via activation of a β_3-adrenoceptor–dependent pathway, thus blunting gain in body weight and adiposity during HFD (Figure 8). While we cannot exclude a role of ROS in metabolic processes in other regions of the brain, our findings reveal a potentially novel role for hypothalamic oxidative stress in modulating β_3-adrenoceptor signaling in the development of obesity, with the hypothalamic PVN playing a pivotal role.

Methods

Animals. All studies were performed on male mice harboring a conditional allele of *p22*^{phox} (*p22*$^{phox/fl}$) (23) obtained from David G. Harrison (Vanderbilt University, Nashville, Tennessee, USA) and used to establish our own colony. Mice were fed an NC diet until the start of experimental procedures and were singly housed with a 12-hour light/dark cycle. All studies were conducted according to procedures approved by the Cornell University IACUC.

Adenoviral targeting of p22^{phox} *to the PVN*. Six-week-old *p22*$^{phox/fl}$ mice underwent microinjection of an adenovirus encoding Cre-recombinase (AdCre, 4×10^{10} plaque-forming units/ml) or titer-matched LacZ (AdLacZ) bilaterally into the PVN as described (43). We used adenovirus as the gene transfer vector since NADPH oxidase is expressed in both neurons and glia, and this virus targets both cell types (59, 60). Briefly, mice were anesthetized (ketamine 150 mg/kg + xylazine 15 mg/kg, i.p.) and placed in a stereotaxic device (Stoelting). After drilling a hole in the appropriate skull location, AdCre or AdLacZ was injected bilaterally into the PVN using a glass micropipette (coordinates: –0.7 mm bregma, ± 0.2 mm midline, 4.6 mm dorsal). Mice were given 7–10 days for recovery to allow for viral expression before the start of HFD. We and oth-

Table 1. Target genes and primer sequences for quantitative rtPCR

Target Gene	Primer Sequence
18S:	F: 5′-GTAACCCGTTGAACCCCATT-3′ R: 5′-CCATCCAATCGGTAGTAGCG-3′
p22^{phox}:	F: 5′-TCCCATTGAGCCTAAACCCAAGGA-3′ R: 5′-ACGACCTCATCTGTCACTGGCATT-3′
Ucp-1:	F: 5′-TGAAGGTCAGAATGCAAGCCCA-3′ R: 5′-TGACAAGCTTTCTGTGGTGGCT-3′
Pgc-1α:	F: 5′-AAGCAATTGAAGAGCGCCGTGT-3′ R: 5′-TCCCGCAGATTTACGGTGCATT-3′
Adrb3:	F: 5′-TCCACCGCTCAACAGGTTTGAT-3′ R: 5′-TGCATCCATAGCCGTTGCTTGT-3′
Hsl:	F: 5′-GGCTTACTGGGCACAGATACCT-3′ R: 5′-CTGAAGGCTCTGAGTTGCTCAA-3′
Prdm16:	F: 5′-TCATCCCAGGAGAGCTGCATCAAA-3′ R: 5′-ATCACAGGAACACGCTACACGGAT-3′

ers have shown previously that adenoviral gene transfer to various brain regions including the PVN results in robust and long-term gene expression (61–63). Furthermore, we have previously shown that Cre-mediated deletion of *p22^{phox}* is permanent in tissues such as the subfornical organ of the brain or vascular smooth-muscle cells (23, 26).

In a separate experiment we investigated whether deletion of PVN *p22^{phox}* has an effect on further weight gain after the onset of obesity. Here, 6-week-old *p22$^{phox/fl}$* mice were placed on HFD for 8 weeks before PVN adenoviral injection and body weight gain was measured for an additional 10 weeks.

Induction of obesity and measurements of locomotor activity, food intake, and energy expenditure. Mice were individually housed and started on a HFD (42% calories from fat, Harlan Tekland) to stimulate DIO. Control cohorts received NC (5 % calories from fat, Harlan Tekland). Food intake was measured weekly over a 24-hour period at the same time each day. A fixed amount of food pellets was weighed, placed in a feeder, and reweighed after mice were in the cage for 24 hours. After 10 weeks of HFD, some cohorts of mice were placed in a Comprehensive Laboratory Animal Monitoring System (CLAMS, Columbus Instruments) for 3 days. After allowing the mice 48 hours to acclimate, energy expenditure, food intake, and locomotor activity were measured over 24 hours. For a subset of studies the β_3-adrenoreceptor antagonist SR59230A (Sigma-Aldrich) was injected i.p. (2 mg/kg, 100 μl, daily) for 3 consecutive days during indirect calorimetry (36).

Quantitative real-time polymerase chain reaction (rtPCR). All brain tissues were removed immediately after decapitation and frozen on dry ice. Micropunches of the PVN, arcuate nucleus, and CTX were isolated using the coordinates of Paxinos and Franklin (64) and methods utilized by our laboratory and others (43, 62). Briefly, brains were embedded in optimal cutting temperature (OCT) freezing medium and coronally cryosectioned in the appropriate location based on anatomical landmarks. A single micropunch (Stoelting) was obtained for the arcuate nucleus (0.25 mm), whereas bilateral micropunches were collected for the PVN (0.5 mm) and somatosensory CTX (0.75 mm). Brain tissue from 2 mice was pooled per biological sample. RNA was extracted using TRIzol reagent according to the manufacturer's protocol (Invitrogen). RNA with an A260/280 ratio between 1.6 and 2.0 was used for reverse transcription with the qScript cDNA kit (Quanta BioSciences). Quantitative rtPCR was performed in triplicate with an ABI 7500 Fast Thermocycler (Applied Bioscience) using SYBR Green (Quanta BioSciences). All rtPCR primers were designed using PrimerQuest from Integrated DNA Technologies (Table 1). Data were analyzed using the ΔΔCt method and expressed as fold change (65). All results were normalized to *18S*.

Measurement of ROS in the brain. DHE fluoroscopy was used to measure ROS in the PVN as described in previous studies (43, 45). After decapitation, brains were immediately frozen on dry ice and covered in OCT mounting medium. Tissue slices (20 μm) were mounted on glass slides and incubated with 2 μmol/l DHE for 5 minutes in the dark. Three slow rinses with phosphate-buffered saline were then performed to wash off excess DHE and images were obtained using a confocal microscope (Zeiss LSM 510) at an excitation wavelength of 488 nm. Control and experimental samples were processed on the same slide in parallel. DHE fluorescence was analyzed using ImageJ software (NIH). The mean DHE fluorescence of the experimental samples was expressed as fold change relative to the paired control sample (AdLacZ NC).

Immunohistochemistry. After euthanasia, mice were perfused with a heparin-containing saline solution (15 minutes) and then with formalin (15 minutes). ScWAT was harvested and stored in 70% ethanol until it was paraffin embedded. H&E staining was performed according to standard procedures. In brief, 5-μm sections of scWAT were obtained and collected on slides. The sections were deparaffinized with a series of xylene and alcohol washes, followed by staining with H&E, and then a final series of alcohol and xylene washes. Slides were coverslipped with Permount mounting medium and imaged with an Olympus BX43 microscope.

NE quantification in adipose tissue. NE was quantified using an ELISA in duplicate according to the manufacturer's protocol (IBL America). Tissues were homogenized by sonication in homogenization buffer as described previously (35), and the clear homogenates were stored at –80°C until further use. The measurements were normalized to the protein concentration of each sample that was determined by a bicinchoninic acid assay.

Data analysis. Data are expressed as the mean ± SEM. To determine statistical significance, we performed a 2-way ANOVA followed by a Sidak multiple comparison post-hoc test for time-course experiments. In all other experiments, a 1-way ANOVA followed by Tukey's post-hoc test was used. *P* values less than 0.05 were considered significant.

Author contributions

HEL, ALM, and RLD designed the studies. HEL, JS, CH, CNY, and AC performed and analyzed the experiments. HEL, ALM, and RLD wrote the paper. JS, CH, CNY, ALM, and RLD participated in important discussions of the data. All authors approved the manuscript.

Acknowledgments

We thank Jen Musa for her assistance with editing the manuscript. This work was supported by NIH grants HL084207 (to R.L.D. and A.L.M.), HL063887 (to R.L.D.), and HL16776 (to C.N.Y.), by an American Heart Association Scientist Development grant 12SDG8790000 (to H.E.L), and by research funds from the Roy J. Carver Trust (to A.L.M).

Address correspondence to: Robin L. Davisson, T9-014C Veterinary Research Tower, Cornell University, Ithaca, New York 14853-6401, USA. Phone: 607.253.3598; E-mail: robin.davisson@cornell.edu.

1. Spiegelman BM, Flier JS. Obesity and the regulation of energy balance. *Cell*. 2001;104(4):531–543.
2. Cone RD. Anatomy and regulation of the central melanocortin system. *Nat Neurosci*. 2005;8(5):571–578.
3. Ferguson AV, Renaud LP. Hypothalamic paraventricular nucleus lesions decrease pressor responses to subfornical organ stimulation. *Brain Res*. 1984;305(2):361–364.
4. Amir S. Stimulation of the paraventricular nucleus with glutamate activates interscapular brown adipose tissue thermogenesis in rats. *Brain Res*. 1990;508(1):152–155.
5. Shi YC, et al. Arcuate NPY controls sympathetic output and BAT function via a relay of tyrosine hydroxylase neurons in the PVN. *Cell Metab*. 2013;17(2):236–248.
6. Cannon B, Nedergaard J. Brown adipose tissue: function and physiological significance. *Physiol Rev*. 2004;84(1):277–359.
7. Rothwell NJ, Stock MJ. A role for brown adipose tissue in diet-induced thermogenesis. *Obes Res*. 1997;5(6):650–656.
8. Madden CJ, Morrison SF. Neurons in the paraventricular nucleus of the hypothalamus inhibit sympathetic outflow to brown adipose tissue. *Am J Physiol Regul Integr Comp Physiol*. 2009;296(3):R831–R843.
9. Trayhurn P, Ashwell M. Control of white and brown adipose tissues by the autonomic nervous system. *Proc Nutr Soc*. 1987;46(1):135–142.
10. Nedergaard J, Cannon B. The browning of white adipose tissue: some burning issues. *Cell Metab*. 2014;20(3):396–407.
11. Boström P, et al. A PGC1-α-dependent myokine that drives brown-fat-like development of white fat and thermogenesis. *Nature*. 2012;481(7382):463–468.
12. Wu J, et al. Beige adipocytes are a distinct type of thermogenic fat cell in mouse and human. *Cell*. 2012;150(2):366–376.
13. Bamshad M, Aoki VT, Adkison MG, Warren WS, Bartness TJ. Central nervous system origins of the sympathetic nervous system outflow to white adipose tissue. *Am J Physiol*. 1998;275(1 Pt 2):R291–R299.
14. Stanley S, et al. Identification of neuronal subpopulations that project from hypothalamus to both liver and adipose tissue polysynaptically. *Proc Natl Acad Sci USA*. 2010;107(15):7024–7029.
15. Foster MT, Song CK, Bartness TJ. Hypothalamic paraventricular nucleus lesion involvement in the sympathetic control of lipid mobilization. *Obesity (Silver Spring)*. 2010;18(4):682–689.
16. Harrison D, Griendling KK, Landmesser U, Hornig B, Drexler H. Role of oxidative stress in atherosclerosis. *Am J Cardiol*. 2003;91(3A):7A–11A.
17. Griendling KK, Sorescu D, Ushio-Fukai M. NAD(P)H oxidase: role in cardiovascular biology and disease. *Circ Res*. 2000;86(5):494–501.
18. Keaney JF, et al. Obesity and systemic oxidative stress: clinical correlates of oxidative stress in the Framingham Study. *Arterioscler Thromb Vasc Biol*. 2003;23(3):434–439.
19. Otani H. Oxidative stress as pathogenesis of cardiovascular risk associated with metabolic syndrome. *Antioxid Redox Signal*. 2011;15(7):1911–1926.
20. De Souza CT, et al. Consumption of a fat-rich diet activates a proinflammatory response and induces insulin resistance in the hypothalamus. *Endocrinology*. 2005;146(10):4192–4199.
21. Zhang X, Zhang G, Zhang H, Karin M, Bai H, Cai D. Hypothalamic IKKbeta/NF-kappaB and ER stress link overnutrition to energy imbalance and obesity. *Cell*. 2008;135(1):61–73.
22. Cai D, Liu T. Hypothalamic inflammation: a double-edged sword to nutritional diseases. *Ann N Y Acad Sci*. 2011;1243:E1–E39.
23. Lob HE, Schultz D, Marvar PJ, Davisson RL, Harrison DG. Role of the NADPH oxidases in the subfornical organ in angiotensin II-induced hypertension. *Hypertension*. 2013;61(2):382–387.
24. Laude K, et al. Hemodynamic and biochemical adaptations to vascular smooth muscle overexpression of p22phox in mice. *Am J Physiol Heart Circ Physiol*. 2005;288(1):H7–H12.
25. Zafari AM, et al. Role of NADH/NADPH oxidase-derived H_2O_2 in angiotensin II-induced vascular hypertrophy. *Hypertension*. 1998;32(3):488–495.

26. Youn JY, Siu KL, Lob HE, Itani H, Harrison DG, Cai H. Role of vascular oxidative stress in obesity and metabolic syndrome. *Diabetes*. 2014;63(7):2344–2355.
27. Nagae A, Fujita M, Kawarazaki H, Matsui H, Ando K, Fujita T. Sympathoexcitation by oxidative stress in the brain mediates arterial pressure elevation in obesity-induced hypertension. *Circulation*. 2009;119(7):978–986.
28. Feldmann HM, Golozoubova V, Cannon B, Nedergaard J. UCP1 ablation induces obesity and abolishes diet-induced thermogenesis in mice exempt from thermal stress by living at thermoneutrality. *Cell Metab*. 2009;9(2):203–209.
29. Surwit RS, et al. Diet-induced changes in uncoupling proteins in obesity-prone and obesity-resistant strains of mice. *Proc Natl Acad Sci USA*. 1998;95(7):4061–4065.
30. Cao L, et al. White to brown fat phenotypic switch induced by genetic and environmental activation of a hypothalamic-adipocyte axis. *Cell Metab*. 2011;14(3):324–338.
31. Seale P, et al. Prdm16 determines the thermogenic program of subcutaneous white adipose tissue in mice. *J Clin Invest*. 2011;121(1):96–105.
32. Uldry M, Yang W, St-Pierre J, Lin J, Seale P, Spiegelman BM. Complementary action of the PGC-1 coactivators in mitochondrial biogenesis and brown fat differentiation. *Cell Metab*. 2006;3(5):333–341.
33. Vaughan M, Berger JE, Steinberg D. Hormone-sensitive lipase and monoglyceride lipase activities in adipose tissue. *J Biol Chem*. 1964;239:401–409.
34. Bamshad M, Song CK, Bartness TJ. CNS origins of the sympathetic nervous system outflow to brown adipose tissue. *Am J Physiol*. 1999;276(6 Pt 2):R1569–R1578.
35. Qiu Y, et al. Eosinophils and type 2 cytokine signaling in macrophages orchestrate development of functional beige fat. *Cell*. 2014;157(6):1292–1308.
36. López M, et al. Hypothalamic AMPK and fatty acid metabolism mediate thyroid regulation of energy balance. *Nat Med*. 2010;16(9):1001–1008.
37. Lassègue B, San Martín A, Griendling KK. Biochemistry, physiology, and pathophysiology of NADPH oxidases in the cardiovascular system. *Circ Res*. 2012;110(10):1364–1390.
38. Fukui T, et al. p22phox mRNA expression and NADPH oxidase activity are increased in aortas from hypertensive rats. *Circ Res*. 1997;80(1):45–51.
39. Oscai LB, Brown MM, Miller WC. Effect of dietary fat on food intake, growth and body composition in rats. *Growth*. 1984;48(4):415–424.
40. Wilson BE, Meyer GE, Cleveland JC, Weigle DS. Identification of candidate genes for a factor regulating body weight in primates. *Am J Physiol*. 1990;259(6 Pt 2):R1148–R1155.
41. Lee P, Brychta RJ, Linderman J, Smith S, Chen KY, Celi FS. Mild cold exposure modulates fibroblast growth factor 21 (FGF21) diurnal rhythm in humans: relationship between FGF21 levels, lipolysis, and cold-induced thermogenesis. *J Clin Endocrinol Metab*. 2013;98(1):E98–E102.
42. Veeneman JM, de Jong PE, Huisman RM, Reijngoud DJ. Re: Adey et al. Reduced synthesis of muscle proteins in chronic renal failure. Am J Physiol Endocrinol Metab. 278: E219-E225, 2000. *Am J Physiol Endocrinol Metab*. 2001;280(1):E197–E198.
43. Infanger DW, et al. Silencing nox4 in the paraventricular nucleus improves myocardial infarction-induced cardiac dysfunction by attenuating sympathoexcitation and periinfarct apoptosis. *Circ Res*. 2010;106(11):1763–1774.
44. Kishi T, Hirooka Y, Kimura Y, Ito K, Shimokawa H, Takeshita A. Increased reactive oxygen species in rostral ventrolateral medulla contribute to neural mechanisms of hypertension in stroke-prone spontaneously hypertensive rats. *Circulation*. 2004;109(19):2357–2362.
45. Zimmerman MC, Lazartigues E, Sharma RV, Davisson RL. Hypertension caused by angiotensin II infusion involves increased superoxide production in the central nervous system. *Circ Res*. 2004;95(2):210–216.
46. Yowtak J, Wang J, Kim HY, Lu Y, Chung K, Chung JM. Effect of antioxidant treatment on spinal GABA neurons in a neuropathic pain model in the mouse. *Pain*. 2013;154(11):2469–2476.
47. Cypess AM, et al. Activation of human brown adipose tissue by a β_3-adrenergic receptor agonist. *Cell Metab*. 2015;21(1):33–38.
48. Consoli D, Leggio GM, Mazzola C, Micale V, Drago F. Behavioral effects of the beta3 adrenoceptor agonist SR58611A: is it the putative prototype of a new class of antidepressant/anxiolytic drugs? *Eur J Pharmacol*. 2007;573(1–3):139–147.
49. Berg T, Piercey BW, Jensen J. Role of beta1-3-adrenoceptors in blood pressure control at rest and during tyramine-induced norepinephrine release in spontaneously hypertensive rats. *Hypertension*. 2010;55(5):1224–1230.
50. Summers RJ, Papaioannou M, Harris S, Evans BA. Expression of beta 3-adrenoceptor mRNA in rat brain. *Br J Pharmacol*. 1995;116(6):2547–2548.
51. Koller KJ, Wolff RS, Warden MK, Zoeller RT. Thyroid hormones regulate levels of thyrotropin-releasing-hormone mRNA in the paraventricular nucleus. *Proc Natl Acad Sci USA*. 1987;84(20):7329–7333.
52. Filaretov AA, Filaretova LP. Role of the paraventricular and ventromedial hypothalamic nuclear areas in the regulation of the pituitary-adrenocortical system. *Brain Res*. 1985;342(1):135–140.
53. Marvar PJ, et al. T lymphocytes and vascular inflammation contribute to stress-dependent hypertension. *Biol Psychiatry*. 2012;71(9):774–782.
54. Shin AC, et al. Chronic exposure to a high-fat diet affects stress axis function differentially in diet-induced obese and diet-resistant rats. *Int J Obes (Lond)*. 2010;34(7):1218–1226.
55. Nillni EA. Regulation of the hypothalamic thyrotropin releasing hormone (TRH) neuron by neuronal and peripheral inputs. *Front Neuroendocrinol*. 2010;31(2):134–156.
56. Tannenbaum BM, Brindley DN, Tannenbaum GS, Dallman MF, McArthur MD, Meaney MJ. High-fat feeding alters both basal and stress-induced hypothalamic-pituitary-adrenal activity in the rat. *Am J Physiol*. 1997;273(6 Pt 1):E1168–E1177.
57. Dallman MF, la Fleur SE, Pecoraro NC, Gomez F, Houshyar H, Akana SF. Minireview: glucocorticoids--food intake, abdominal obesity, and wealthy nations in 2004. *Endocrinology*. 2004;145(6):2633–2638.
58. Perello M, et al. Maintenance of the thyroid axis during diet-induced obesity in rodents is controlled at the central level. *Am J Physiol Endocrinol Metab*. 2010;299(6):E976–E989.
59. Abramov AY, Jacobson J, Wientjes F, Hothersall J, Canevari L, Duchen MR. Expression and modulation of an NADPH oxi-

dase in mammalian astrocytes. *J Neurosci*. 2005;25(40):9176–9184.
60. Tammariello SP, Quinn MT, Estus S. NADPH oxidase contributes directly to oxidative stress and apoptosis in nerve growth factor-deprived sympathetic neurons. *J Neurosci*. 2000;20(1):RC53.
61. Tripathy SK, Black HB, Goldwasser E, Leiden JM. Immune responses to transgene-encoded proteins limit the stability of gene expression after injection of replication-defective adenovirus vectors. *Nat Med*. 1996;2(5):545–550.
62. Burmeister MA, Young CN, Braga VA, Butler SD, Sharma RV, Davisson RL. In vivo bioluminescence imaging reveals redox-regulated activator protein-1 activation in paraventricular nucleus of mice with renovascular hypertension. *Hypertension*. 2011;57(2):289–297.
63. Peterson JR, et al. Longitudinal noninvasive monitoring of transcription factor activation in cardiovascular regulatory nuclei using bioluminescence imaging. *Physiol Genomics*. 2008;33(2):292–299.
64. Paxinos G Franklin KBJ. *The Mouse Brain in Stereotaxic Coordinates*. Amsterdam; Boston: Elsevier Academic Press; 2004.
65. Livak KJ, Schmittgen TD. Analysis of relative gene expression data using real-time quantitative PCR and the 2(-Delta Delta C(T)) Method. *Methods*. 2001;25(4):402–408.